Controlling the morphology of electrospray-generated PLGA microparticles for drug delivery

Begoña Almería [a], Weiwei Deng [a], Tarek M. Fahmy [b], Alessandro Gomez [a,*]

[a] Department of Mechanical Engineering, Yale University, New Haven, CT 06520-8286, USA
[b] Department of Biomedical and Chemical Engineering, Yale University, New Haven, CT 06520-8286, USA

A B S T R A C T

We developed a well-controlled method to generate PLGA microparticles of different morphologies using the electrospray drying route. By judiciously selecting polymer molecular weight, concentration, and solution flow rate, we can control the order in which polymer entanglements and Coulomb fission occur in the droplets and their relative importance, and subsequently govern the morphology of the resulting polymer particles. We show that spherical, monodisperse particles are generated when sufficiently strong polymer entanglements set in the evaporating droplets *before* they undergo any Coulomb fission. On the other hand, tailed and elongated particles are obtained if the Coulomb fission occurs first and if the droplets/particles are sufficiently evaporated to freeze in their irregular shape. Strictly spherical particles are unachievable for polymer solutions below a critical concentration, because the onset of Coulomb fission always sets in prior to the development of a sufficiently entangled polymer network. An extension of a simple model, originally used to determine the onset of electrospinning of polymer solutions, adequately predicts when non-spherical particles are produced. We conclude by demonstrating the scale-up of this approach to the synthesis of polymer particles using a compact, microfabricated, multiplexed electrospray system, which would make it suitable for practical applications.

© 2009 Elsevier Inc. All rights reserved.

1. Introduction

Solid biodegradable micro- and nanoparticles are of considerable interest for therapeutic development for several reasons. First, in addition to their small size, they can solubilize a concentrated payload of drug, improve drug stability and bioavailability, and extend drug or gene effect through sustained delivery. Moreover, the use of biodegradable, biocompatible materials reduces the risk of unwanted toxicities and adverse effects. Finally, these systems have proven to be versatile platforms for the delivery of a large variety of compounds, ranging from small molecules to larger macromolecules such as proteins and oligonucleotides.

Among the variety of materials available to engineer these solid particles, the most widely used are the aliphatic polyesters, specifically poly (lactic acid) (PLA), poly (glycolic acid) (PGA) and their copolymer, poly (lactide-co-glycolide) (PLGA) [1–4]. Recent advances in the design of these type of drug deliverers have included modification of the particle surface to improve stability and circulation throughout the body [5], biospecific targeting against cellular ligands or extracellular matrix components [6–9], and incorporation of diagnostic imaging agents [10].

Engineering particles with diverse morphologies is becoming increasingly important, since recent studies have proved that morphology influences the mechanisms of drug delivery in many ways [11,12]. First, it affects the degradation of the polymer matrix and thus the kinetics of the drug release. An appropriate shape can therefore help tailor the drug release profile, and even avoid the initial burst [13]. Second, transport and circulation of polymer particles inside the body are also highly influenced by morphology. For example, compared to spherical particles, it is easier for elongated ones to align with the flow, and therefore travel through tortuous pathways in organs or tissues with fewer collisions [14,15]. Third, the particle morphology, and particularly the local shape at the binding site, dictates clearance of particles by macrophage internalization [16]. Internalization by non-phagocytic cells is also shape-dependent, and particles with high aspect ratio are internalized up to three times faster than their spherical counterparts [17]. Finally, the particle local curvature will also determine its targeting ability, that is, delivering the encapsulated drug to specific cells, by affecting the attachment of targeting ligands to the receptors in the cell membrane [11]. Different morphologies result in different affinities of anchoring on targeted cells, which explains why disk-shaped particles are three times more effective than spherical particles [18]. Particles with large surface-to-volume ratio are also preferred for targeting, since large surfaces allow for the conjugation of numerous ligands.

With the ultimate goal of exploiting the advantages brought by different morphologies, we developed a new method to generate PLGA particles that are elongated, stretched, or of even more complex shape in a controlled fashion using the electrospray (ES) drying route. Previous work on electrospray drying of PLGA and other polymers in solution mainly focused on achieving spherical and monodisperse particles [19–28]. Unlike the particle size, which can be easily tuned by adjusting flow rate and polymer concentration [20–23], the control of particle shape is a more challenging task. To date, only three morphologies (spheres, shells and doughnuts) have been achieved through the competition between solvent evaporation and polymer diffusion within the droplets [21,24–27]. A systematic study of the effect of polymer concentration and solution flow rate on particle morphology has recently been carried out in [28]. However, a general explanation of the processes from first principles and a generalized discussion that is not restricted to a particular combination of solvent–polymer is still missing.

In this paper, we first present a ES-based methodology to generate differently shaped particles based on knowledge of properties of the polymer solution and flow rate. Then, we extend the model developed by Shenoy et al. [29] in a different context to predict the (spherical versus irregular) morphology of the generated polymer particles. We conclude by demonstrating that the drawback of low-throughput of the electrospray drying method is overcome by using a compact, microfabricated, multiplexed electrospray system, with a scale-up potential of several orders of magnitude.

2. Materials and methods

2.1. Materials

Several polymer solutions with polymer volume fractions ranging from 0.015 to 0.082 (2–12%w/v, respectively) were prepared by dissolving ester-terminated PLGA (50:50) (IV 0.55–0.75, M_w = 53.8 kDa, Lactel Absorbable Polymers, Durect Corporation) in 2,2,2-trifluoroethanol (TFE, Reagent Plus grade, purity ⩾99%, Sigma–Aldrich). A small amount (0.05% by weight with respect to the weight of polymer in solution) of Rhodamine B (Acros Organics) was added as a surrogate of an active agent, with the intention of monitoring its release rate from the polymer particles when suspended in an aqueous solution. The surrogate drug release study will be addressed in separate work.

The most relevant solution properties that affect the electrospray generation of polymer particles are evaporation rate, density, electrical conductivity, surface tension, viscosity, dielectric constant, and polymer concentration, as extensively demonstrated through [19–28]. Table 1 summarizes the measured values for these parameters. Surface tension (γ) was measured using the cap-

illary method. Electrical conductivity (k) was inferred by measuring the electric current passing through a column of liquid of known dimensions connecting two opposite electrodes at different voltages. Viscosity measurements were performed using an AR2000 Rheometer from TA Instruments. The dielectric constant (ε) of the solutions is expected to be close to that of TFE at 26.01. Therefore, it has negligible influence on the characteristics of the generated particles [30]. Neither PLGA nor Rhodamine were found to affect the surface tension of the polymer solutions. The electrical conductivity of TFE–PLGA solutions decreased with the increasing polymer concentration. However, this trend was reversed once Rhodamine was added to the mixture, because the concentration of Rhodamine, whose conductivity is higher than TFE, also increases. The viscosity of the solutions (μ) increased linearly with the polymer concentration. Even so, the viscosity in the jet break up is too low to affect the established ES scaling laws [30–32].

2.2. Experimental setup

PLGA particles with controlled morphology and size were produced using a single electrospray source (Fig. 1a) as well as a microfabricated, multiplexed electrospray (MES) device consisting of several electrospray sources operating in parallel (Fig. 1b). For the single electrospray source, we used a stainless steel capillary with an outer diameter of either 210 μm or 500 μm. The capillary was maintained at several kilovolts with respect to a grounded plate, and a syringe pump supplied the polymer solution through the capillary. For the multiplexed electrospray sources, we used a microfabricated MES device consisting of a silicon nozzle chip and an extractor. The technical details of the MES device are documented in [33,34]. Briefly, the chip comprises several electrospray nozzles arranged in a hexagonal pattern. For this study, we used two different chips with 7 and 19 sources. These sources, with outer and inner diameters of 210 μm and 60 μm respectively, protrude 450 μm from the base of the chip, and have a pitch (distance between two adjacent nozzles) of 675 μm. The nozzle chip is mounted on a liquid reservoir, which serves the dual function of distributing the liquid homogeneously among all nozzles and providing the electrical contact to supply ~11 kV to the liquid. An extractor electrode, with an array of 400 μm diameter circular openings that are aligned with the nozzles, is separated from the chip by a 300 μm Pyrex® sheet insulating spacer.

A voltage drop of approximately 2 kV between the nozzle chip and the extractor provides the electric field needed to generate the electrosprays. A second ring electrode, charged at 7 kV, is placed 7 mm below the extractor, and 7 cm above the grounded silicon collecting plate. The ring electrode helps to accelerate the particles towards the collector. Otherwise, an excessively large voltage difference would be needed between the extractor and the collector to prevent the droplets from flying back to the

Table 1
Solutions properties relevant for their atomization: ϕ, polymer volume fraction; ρ, density; k, electrical conductivity; γ, surface tension; and μ, viscosity.

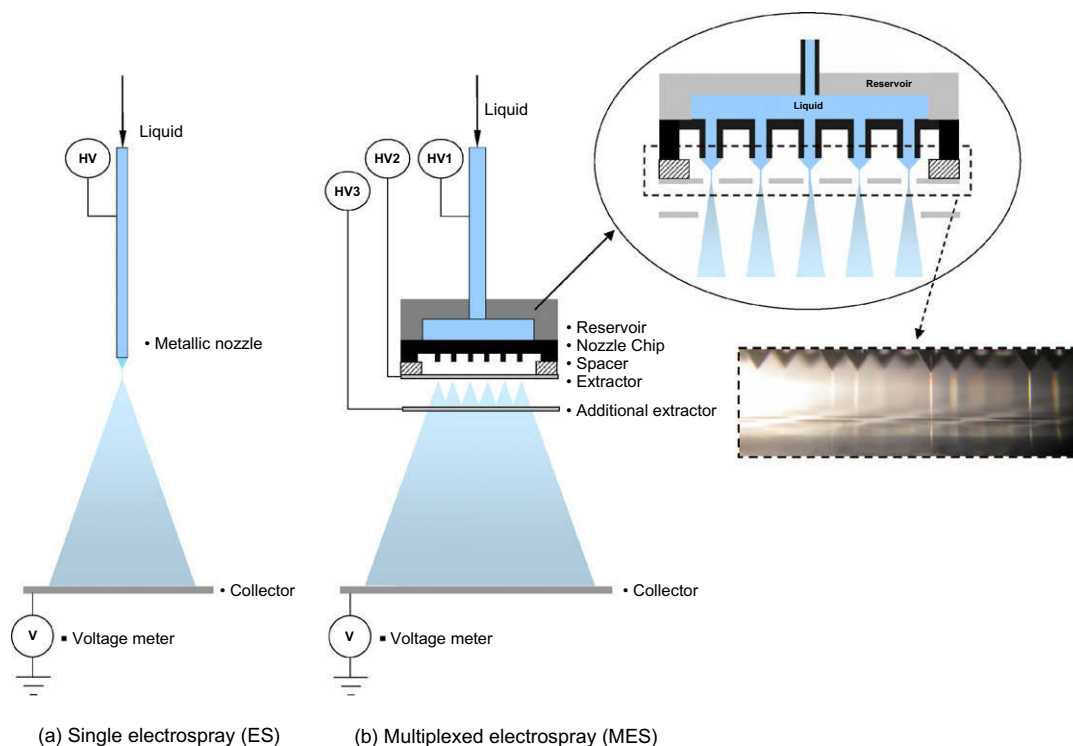|	ϕ	ρ (g/ml)	$k * 10^4$ (S/m)	γ (dyn/cm)	μ (Cp)
TFE		1.373	1.420	18.925	1.500
PLGA (50:50), M_w = 53, 8.7 kDa					
With 0.05%w Rhodamine	0.015	1.373	2.066	19.883	4.566
	0.029	1.372	2.229	19.243	7.502
	0.043	1.372	2.521	19.670	11.807
	0.056	1.371	2.630	19.483	16.074
	0.069	1.371	3.122	19.357	20.900
	0.082	1.370	3.287	19.850	22.667
Without Rhodamine	0.015	1.373	1.033		
	0.029	1.372	0.962		
	0.043	1.372	0.915		
	0.056	1.371	0.837		
	0.069	1.371	0.696		

Fig. 1. Single and multiplexed electrospray setup.

extractor [35]. The ring electrode also concentrates the spray "footprint" and thus reduces the particle-coated area on the collector.

The collected particles were imaged with a scanning electron microscope (SEM). The resulting micrographs were analyzed using Image J (NIH) to determine the mean diameter and relative standard deviation of the particle populations.

3. Results and discussion

3.1. Effects of chain entanglements and of Coulomb fission on particle morphology

The controlled generation of polymer particles from solutions entails the competition of solvent evaporation from the surface of the droplets and polymer diffusion, since these polymer particles are the relics obtained after solvent evaporation from the precursor spray droplets [21,24–27]. While a faster evaporation will cause the appearance of porous, hollow, and even fragmented particles, sufficiently rapid polymer diffusion inside the droplets ensures the generation of dense, solid particles. The polymer–solvent combination of the present experiments was chosen so that the latter condition applies, and that complete drying of the particles occurs before they reach the collector. However, contrary to general belief, the dense particles that are generated under these conditions are not necessarily spherical. In fact, two other mechanisms, apart from solvent evaporation and polymer diffusion, contribute to the final particle morphology: chain entanglements and Coulomb fission.

Chain entanglements in polymer melts and solutions are the physical interlocking of the polymer chains, which is a direct consequence of chain overlap. These physical junctions, that cause the onset of fiber formation in electrospinning [29], can preserve both monodispersity and sphericity of the droplet residues by inhibiting Coulomb fission. The latter refers to the process by which a charged droplet emits a cloud of small but highly charged off-

springs droplets [36]. This phenomenon occurs when a charged drop approaches the Rayleigh limit [37], at which the drop cannot hold more charge than a limiting value determined by the balance between the electric stress and surface tension. Droplets generated by the electrospray are likely to undergo Coulomb fission during evaporation, because they shrink without losing charge and eventually reach the Rayleigh limit.

Festag et al. [38] were the first to report that the disintegration of the droplets can be avoided with certain polymer concentrations if entanglements are present *before* the Rayleigh limit is reached, since the energy of the fission process is not sufficient to separate the entangled chains [39]. This fact was later confirmed by Hong et al. [22] and Hogan et al. [23]. However, these authors did not discuss the possible effect of chain entanglements on the *morphology* of the generated particles.

Fig. 2 shows a close-up view of the different morphologies that can be obtained in the electrospray synthesis of polymer particles, some of which were already seen in [40,41], though no connection with the interplay of Coulomb fission and chain entanglements was made. Particles that are spherical (Fig. 2a), elongated (Fig. 2b), with complex shape, with one (Fig. 2c and d) or multiple (Fig. 2e) fibers attached to the particle core, can be obtained.

The appearance of these complex shapes is tentatively explained as follows: if, during the evaporation process, entanglements are present *before* the Rayleigh limit is reached, the electrospray droplet cannot deform or disrupt by Coulomb fission, and the polymer residues will be spherical. If, on the other hand, fission takes place, it tends to deform the particle into other irregular shapes [36] that may relax to the spherical one if the droplet is still in a liquid state. Alternatively, if the droplet evaporation is close to being complete, the droplet/particle may remain frozen in the shape at the time of fission. Under the present conditions, particles of irregular and complex shape, mixed with bidisperse spherical ones, may be produced.

Fig. 3 summarizes these processes as the outcome of three possible scenarios for the evolution of a charged droplet of a dilute
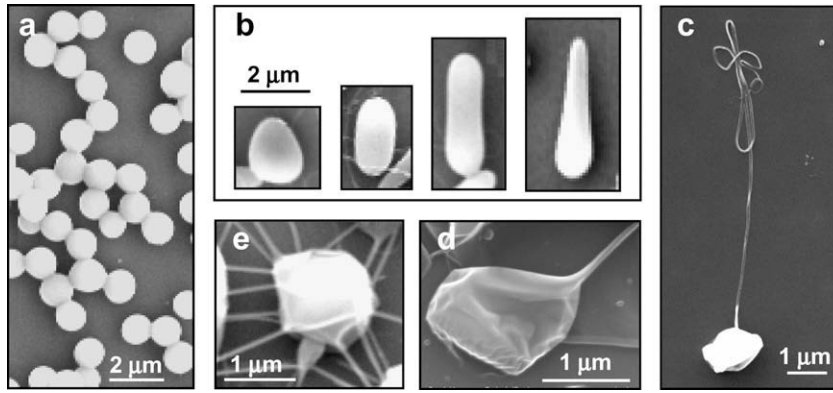
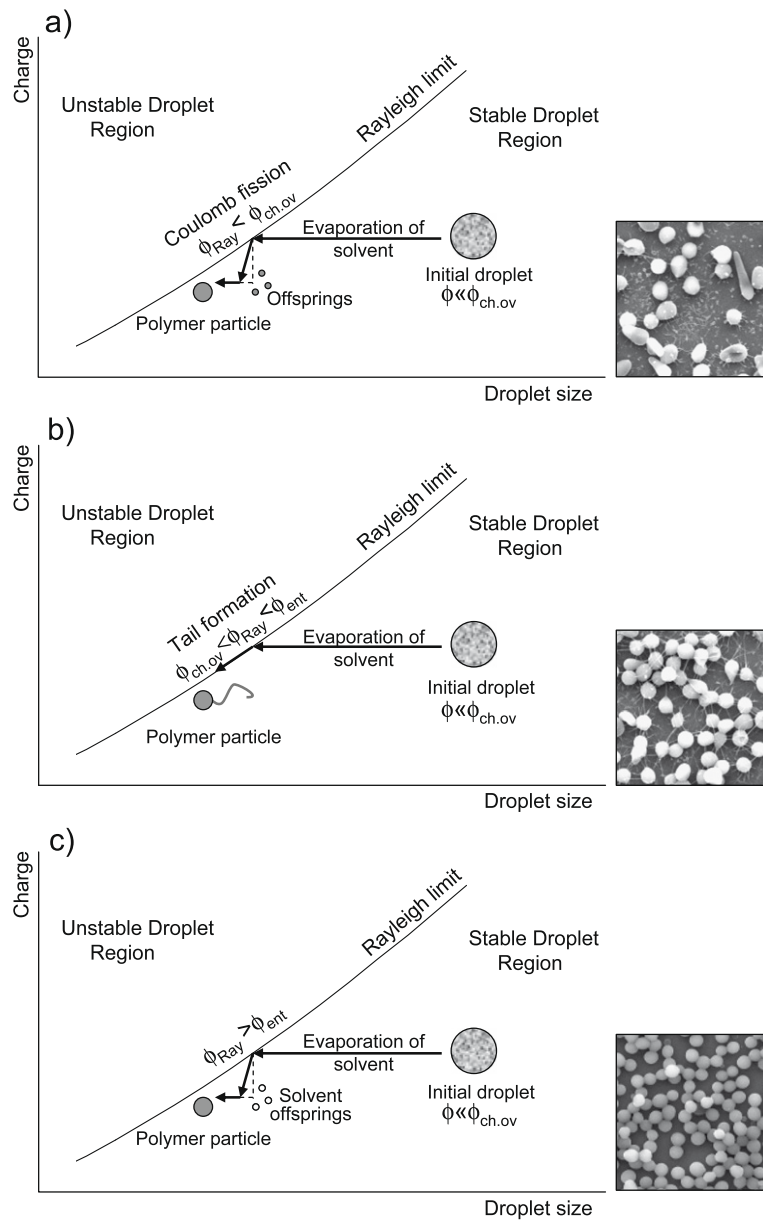**Fig. 2.** Diverse morphologies obtained in PLGA particles.

Fig. 3. Effect of the competition between entanglement and Coulomb fission on particle morphology.

polymer solution undergoing solvent evaporation. The competing mechanisms of Coulomb fission and chain entanglements can yield different outcomes, depending on the relative magnitude of the polymer volume fraction in a droplet at the Rayleigh limit, ϕ_{Ray}, the overlap volume fraction, $\phi_{ch.ov}$, corresponding to conditions when the average distance between chains is on the same order as their size, and the entanglement volume fraction, ϕ_{ent}, at which the polymer volume fraction in the droplets is sufficiently large to form an entangled network of polymer chains. Clearly, $\phi_{ch.ov} < \phi_{ent}$. If $\phi_{Ray} < \phi_{ch.ov}$, the droplet is still sufficiently dilute to behave like a pure liquid (Fig. 3a). In this case, the droplet undergoes Coulomb fission, and small but highly charged offsprings are ejected from the parent droplet, broadening the size distribution of the quasi-spherical particles. If $\phi_{Ray} > \phi_{ent}$, polymer chains will have entangled by the time the droplet reaches its Rayleigh limit, increasing the droplet effective surface tension. The entangled network will therefore stabilize the droplet against rupture, and the particles will remain monodisperse and spherical (Fig. 3c). Alternatively, Coulomb fission may still occur with only solvent offsprings being ejected, but no mass of polymer being emitted, in which case no relics of the offspring would be found in the SEM micrographs.

A most interesting, though so far overlooked, scenario is the intermediate one, that is, $\phi_{ch.ov} < \phi_{Ray} < \phi_{ent}$ (Fig. 3b). This partially entangled polymer network is sufficiently strong to preserve the droplet integrity, but too weak to prevent the particle from deforming via stretching during the fission process. As a result, the particle deforms and a thin and long charged fiber is extruded from it. If the evaporation process is nearly complete, it remains frozen in that shape, as observed in the SEM micrographs.

As a particular case, elongated particles as those shown in Fig. 2b, can be generated when the Rayleigh limit is reached at a late stage in the evaporation process, which "freezes" the stretched particle morphology before the ejection of mass [36]. Depending on the extent of stretching reached by the droplet before complete evaporation, particles with different aspect ratio can be obtained.

3.2. Morphology transition from spherical to non-spherical shapes

Shenoy et al. [29] developed a semi-empirical model to predict the transition from electrospray to electrospinning using the *entanglement number in solution*, $n_{e|sol}$. This number is defined as the ratio of the molecular weight of the polymer, M_w, to the entanglement molecular weight in solution, $M_{e|sol}$. The latter can be expressed as the entanglement molecular weight of the melt, M_e (the molecular weight between polymer junctions), divided by the polymer volume fraction in solution ϕ, that is

$$n_{e|sol} = \frac{M_w}{M_{e|sol}} = \frac{\phi M_w}{M_e}. \tag{1}$$

Three different regimes in the electrospray of polymer solutions were described in [29]: for $n_{e|sol} < 2$, at the onset of chain overlap, regular electrospray was observed; for $n_{e|sol} > 3.5$, electrospinning appeared, and it was attributed to the onset of a sufficiently strong elastic network that stabilizes the jet against breakup; and for $2 < n_{e|sol} < 3.5$, a transitional, mixed regime yielding beads and fibers took place.

Based on the observations in [42], we may regard Coulomb fission as a quasi-steady process similar to that of a stable electrified cone-jet but supported on the droplet instead of the usual capillary tube. Then, we can extend the approach in [29] to predict the morphology of the particles generated by determining whether entanglements in the droplet are present at the Rayleigh limit.

Specifically, setting

$$\phi_{ch.ov} = \phi_{n_{e|sol}=2} = 2\frac{M_e}{M_w} \quad \text{and} \quad \phi_{ent} = \phi_{n_{e|sol}=3.5} = 3.5\frac{M_e}{M_w}, \tag{2}$$

we can compare these values with the polymer volume fraction in the droplet at the moment it reaches the Rayleigh limit, ϕ_{Ray}, and verify if the three scenarios shown in Fig. 3 are properly reproduced. The value of ϕ_{Ray} can be estimated by assuming that the evaporation process occurs without loss of polymer mass. Namely,

$$\phi_{Ray} = \phi\left(\frac{d}{d_R}\right)^3, \tag{3}$$

where d is the initial droplet diameter, and d_R is the droplet diameter at the Rayleigh limit [37], that is,

$$d_R = \left(\frac{q^2}{8\pi^2 \varepsilon \varepsilon_{air} \gamma}\right)^{1/3}, \tag{4}$$

where q is the droplet charge. Assuming uniform size and charge for all the droplets in the spray, we can express the average droplet charge density as the ratio of the current carried by the spray (I) to the corresponding liquid flow rate (Q). Eq. (4) can be rewritten as

$$\phi_{Ray} = \phi\frac{288\varepsilon\varepsilon_{air}\gamma}{\left(\frac{I}{Q}\right)^2 d^3} \tag{5}$$

where ϕ, γ and ε depend exclusively on the polymer solution being used, and I/Q and d can be determined as a function of Q and the solution properties. Since $\phi_{n_{e|sol}=2}$ and $\phi_{n_{e|sol}=3.5}$ also depend solely on the properties of the polymer, namely, on its molecular and entanglement molecular weights, we can predict particle morphology a priori, given polymer solution composition, its physical properties and ES operating conditions (i.e., flow rate). We note, however, that this approach cannot predict detailed morphological features, such as aspect ratio of the elongated particles and length, thickness or number of fibers, but merely sort out spherical from non-spherical products.

3.3. Experimental validation

To validate the methodology presented for the control and prediction of particle morphology, we need to estimate M_e. To that end, we combined Eq. (1) with the value of $\phi_{n_{e|sol}=2}$ obtained experimentally by electrospraying several PLGA solutions with increasing polymer concentration until the appearance of the mixed regime. Its value was bracketed as 1.967 kDa $< M_e <$ 2.917 kDa , which yielded from Eq. (2) $0.073 < \phi_{ch.ov} < 0.108$ and $0.128 < \phi_{ent} < 0.189$. ϕ_{Ray} was estimated using Eq. (5).

Subsequently, PLGA microparticles were synthesized by electrospraying several PLGA–TFE–Rhodamine solutions. We varied the polymer volume fraction from $\phi = 0.015$ to $\phi = 0.082$ at different flow rates. Fig. 4 is a compendium of the morphologies observed in the synthesized particles. The SEM pictures obtained for each solution at different flow rates are superimposed to dashed, constant-ϕ lines. We can divide the figure in three regions, each of them corresponding to a different regime:

- The first region ($\phi > 0.069$) is the *mixed regime,* where beads and fibers are indistinctly generated from the jet. Polymer solutions in this region are so concentrated that cannot be regularly electrosprayed, and neither the processes described in Section 3.1 nor our model apply here.
- The second region ($0.029 < \phi < 0.069$, shaded area in Fig. 4) is the optimal operational regime, where a good control over morphology is achievable. Particle sphericity (case c) in Fig. 3 is preserved as long as $\phi_{Ray} > 0.170$; tailed and elongated particles (case b) are generated when $0.085 < \phi_{Ray} < 0.170$; and, off-springs (case a) appear for $\phi_{Ray} < 0.085$. These experimental observations set values for $\phi_{ch.ov}$ and ϕ_{ent} at 0.085 and 0.170 as marked by the horizontal dashed lines, in the figure. These
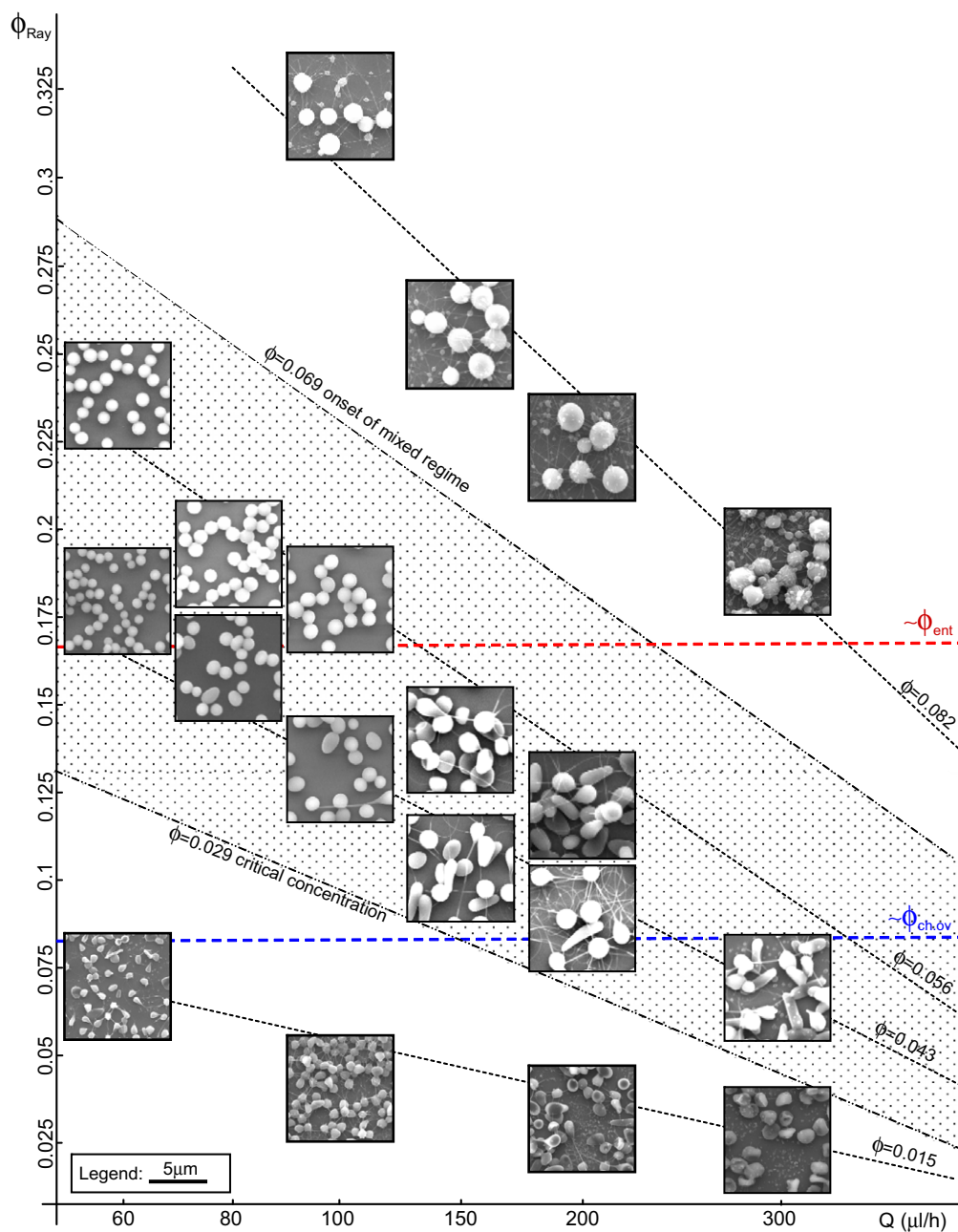
Fig. 4. Overview of PLGA particles synthesized for different initial polymer volume fractions: volume fraction of the polymer in the droplet at the Rayleigh limit plotted as a function of the liquid flow rate. Insets are the observed particle morphologies by SEM.

two values fall within the corresponding intervals estimated *a priori* via Eq. (2), validating the model and its capability to predict particle sphericity or lack thereof.

- The third region ($\phi < 0.029$) corresponds to the subcritical regime, where spherical particles are unachievable. Coulomb fission always sets in prior to the formation of sufficiently strong entanglements, and ϕ_{Ray} in this regime is always smaller than $\phi_{ch.ov}$, as in case a in Fig. 3. Tailed particles are mixed with polydisperse spherical populations as a result of secondary fissions. In fact, the estimated ϕ_{Ray} corresponds to the first time that the droplet reaches the Rayleigh limit, although a charged evaporating droplet may undergo a number of fissions during its evaporation.

Fig. 4 suggests that the value of ϕ_{Ray}, and therefore the morphology of the synthesized polymer particles, depends on both flow

rate and polymer volume fraction. Larger flow rates lead to smaller ϕ_{Ray}, which favors synthesis of complex particles. Higher polymer concentrations, however, tend to preserve particle sphericity at higher flow rates.

Similar behavior was also observed for pure PLGA particles without Rhodamine (see Supplementary material Fig. S9 and Table S2). These results can be also generalized to when real active agents, as opposed to the Rhodamine surrogate, are present.

The opposite effect of flow rate and polymer volume fraction on particle sphericity derived from Eq. (5) can be explained after introducing the dependence of droplet average charge density (I/Q) and diameter (d) on ϕ and Q. While a change in polymer volume fraction ϕ has little effect (through a change in electrical conductivity, see Table 1) on these two parameters, a change in flow rate has a significant impact. For a given polymer solution, I/Q

and d scale as $I/Q \propto Q^{\alpha}$ and $d \propto Q^{\beta}$, where α and β are constants that can be determined either experimentally or using established ES scaling laws [30–32]. Then, according to Eq. (5), $\phi_{Ray} \propto \phi \cdot Q^{2\alpha-3\beta}$. Fig. 5 shows the average droplet charge per unit volume (left) and the droplet diameter (right), as inferred from the residues measurements and knowledge of the solution concentration, as a function of solution flow rate. In our case, $\alpha \leqslant -1/2$ and $\beta \sim 1/3$, and therefore, for a fixed Q, ϕ_{Ray} will decrease as ϕ increases, and for a fixed ϕ, ϕ_{Ray} will increase as Q increases. The value of α stems from the impossibility of the droplets to be charged above the Rayleigh limit [36,43]. On the other hand, β was determined by first estimating the droplet size from the particle diameter measurement with $d = d_p\phi^3$ (where d_p is the particle diameter), and then fitting the resulting data to a power law. Its value of $\sim 1/3$ is within 10% of that from ES scaling laws [30–32] (see Supplementary material Table S3). This agreement with the cited scaling laws was already confirmed in [23], although it contradicts the results shown in [19–22,26] that set the value of β close to ½.

Independent evidence of Coulomb fission, in addition to that offered by the SEM photographs of dry shapes, was obtained by measuring the velocity distributions of the droplets in the spray using a Phase Doppler Particle Analyzer (PDPA), and by following a procedure similar to [36]. We focused on conditions corresponding to the lower right corner of Fig. 4, which should yield offsprings. Fig. 6 shows the velocity–size correlation measured for two different polymer solutions at different flow rates and locations along the spray axis, as specified in the legenda. The measurements are performed on the axis to make sure that they reflect the evolution of the primary droplets, as opposed to the satellites that may be generated by the cone-jet. Fig. 6a shows two different "clouds" of data, corresponding to the main flow and the offsprings generated as a result of the fission process. In the main one (droplet sizes from 4 to 8 μm), velocity and size are reasonably correlated, with larger droplets characterized by greater inertia having larger velocities as compared to the smaller ones within this range. In the smallest size range ($d < 1$ μm), we notice another set of data that are attributed to the offsprings showing in some cases considerably lower and, in a few cases, even negative, velocities as a result of the fission. Although size cannot be determined accurately in this range since it is at the lower limit of the PDPA range, the velocity data are accurate. The present conditions, $\phi = 0.015$ and $Q = 500$ μl/h, correspond to the *subcritical regime* shown in Fig. 4.
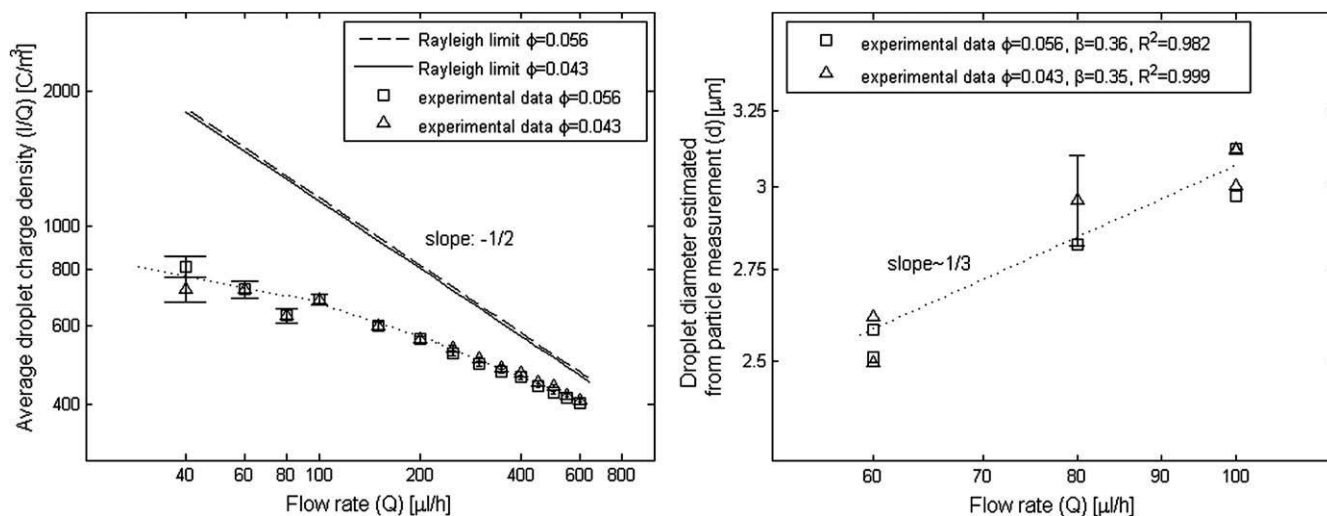

Fig. 5. Dependence of droplet charge density and diameter on flow rate for two values of the polymer volume fraction. The standard deviation is shown as error bars. For clarity, only one representative error bar has been plotted in the right figure.
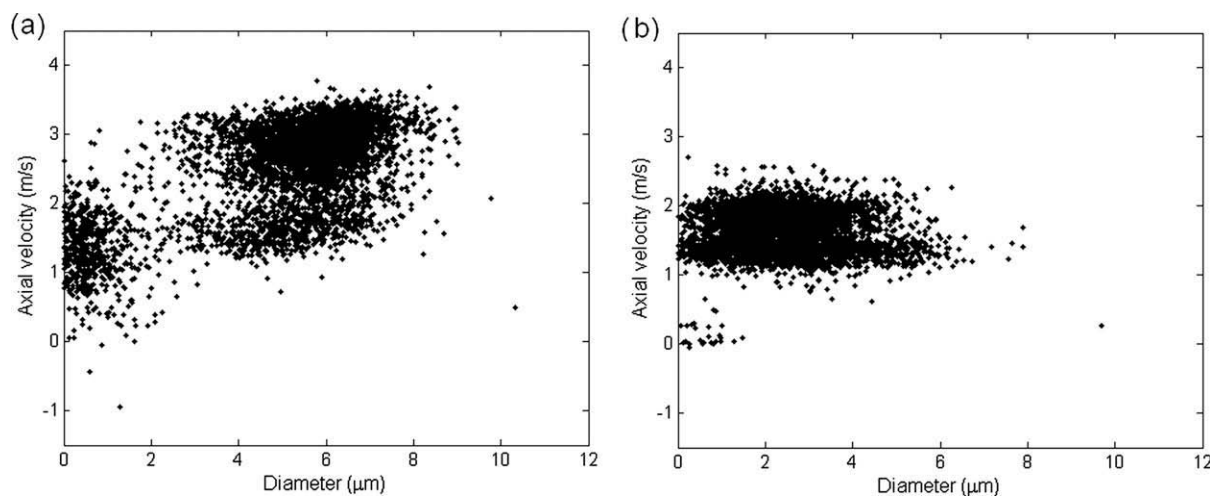

Fig. 6. Velocity–size correlations from PDPA for two different polymer solutions: (a) $\phi = 0.015$, $Q = 500$ μl/h, $z = 2$ cm from jet; (b) $\phi = 0.043$, $Q = 300$ μl/h, $z = 3$ cm from jet.

Fig. 6b corresponds to the case $\phi = 0.043$, $Q = 300$ μl/h, shown in Fig. 4 as part of the lower right corner of the band of *optimal operational regime*. Here, sporadic evidence of Coulomb fissions appears further along the spray axis and a much smaller cloud of offsprings with axial velocity close to zero is detected, corresponding to ejections of offsprings (see SEM micrograph in Fig. 4). No other evidence of Coulomb fission was found in this case or when more concentrated solutions were used, suggesting that the extrusion of fibers from the droplets when they reach the Rayleigh limit does not affect their velocity. In passing, we note that the velocity distribution for the larger droplets appear bimodal, especially in Fig. 6a. A tentative explanation is that the particle velocity is affected by the charge on the droplet, which, in turn, determines the electric force acting on it. This charge varies depending on whether the droplet has undergone one or more fissions, with resulting loss (es) of charge. Thus, the original velocity distribution tends to broaden and may develop bimodality if droplets undergo similar number of fissions.

3.4. Increase of throughput with multiplexed ES

The ES, although successful in the generation of polymer particles of controlled size and morphology suitable for drug delivery, has the well-known shortcoming of low-throughput for practical applications. For example, the typical throughput in the generation of PLGA microparticles is on the order of 0.01 g/h. We overcame this drawback by operating multiple electrospray sources in parallel using a microfabricated MES device (Fig. 1b).

As explained briefly in Section 2.2 and more extensively in [33–35], the design of the multiplexing chip is aimed at ensuring that each individual nozzle in the multiplexed system behaves as if it were isolated. An evenly distributed flow rate to each nozzle, and therefore uniform droplet size, is achieved by letting the viscous pressure drop acting on the liquid across the nozzle dominate over the electrostatic pulling force by the electric field [34]. The presence of the extractor is critical for a successful MES operation because it minimizes the interference between

sources, since the extractor is closer to the nozzle than any neighboring nozzles and therefore the applied electric field is localized. Furthermore, the extractor shields the nozzle tip where the cone-jet is anchored from any electrostatic disturbance that may occur downstream.

We first indirectly confirmed this fact by monitoring the current emitted by the several electrosprays. The total current emitted by the multiplexed device was in excellent agreement with the current emitted by a single-source electrospray working at the same flow rate per source multiplied by the total number of sources on the chip. Direct evidence of the independent performance of each nozzle was obtained by comparing the mean diameters in particle populations generated with both single and multiplexed ES sources operated under same conditions, as Fig. 7 shows. The mean particle agreed within 5% in all but one of the cases (see Supplementary material Table S4), and the standard deviations were below 10% in all cases.

Apart from the spherical particles that were used in Fig. 7 for quantitative comparison, the MES system can also generate particles with the complex morphologies shown for a single electrospray in the previous sections. Fig. 8 shows a compendium of the different shapes generated using a 7-nozzle device to electrospray a TFE–PLGA–Rhodamine solution with polymer volume fraction $\phi = 0.043$. The obtained morphologies reproduce those shown in Fig. 4 for the single electrospray, which verifies the capability of the MES system to reproduce faithfully the results obtained with the single electrospray also in this respect, though with much denser particle populations. Because the performance of single and multiplexed devices is exactly the same, the effect of the flow rate on particle morphology described in Fig. 4 holds for the PLGA particles generated using the multiplexed device. As already discussed, high flow rates such as 200 μl/h favor the synthesis of tailed geometries (Fig. 8a). Particle sphericity correlates inversely to the flow rate, and tails are replaced by rods and spheres as the flow rate is decreased (Fig. 8b and c). Finally, spherical and monodisperse populations are synthesized at sufficiently small flow rates, on the order of 80 μl/h (Fig. 8d).
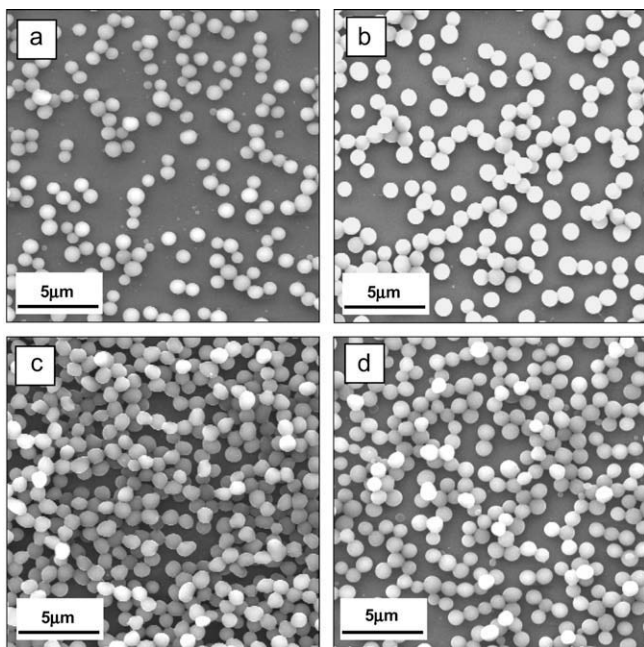

Fig. 7. Comparison between sample obtained by single (a and b) and multiplexed (c and d) ES sources. (a, c) $\phi = 0.043$, Q/nozzle = 70 μl/h; (b, d) $\phi = 0.056$, Q/nozzle = 80 μl/h.
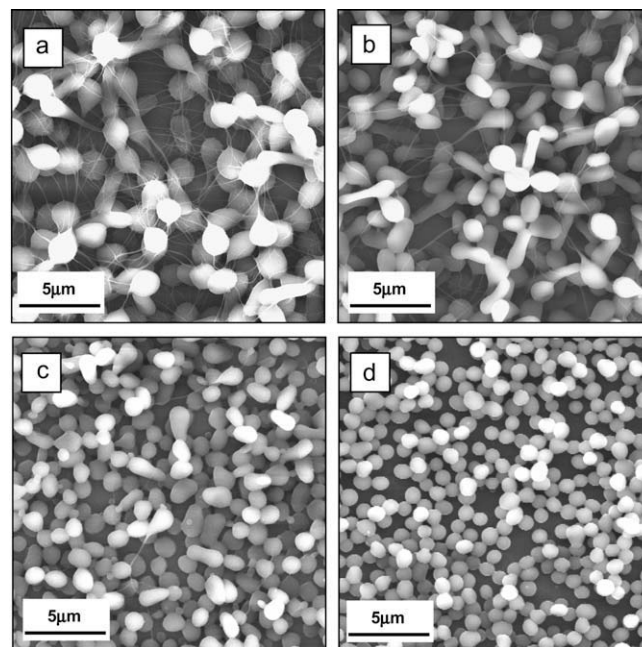

Fig. 8. Overview of PLGA particles synthesized with a 7-nozzles MES device. Solution volume fraction is $\phi = 0.043$. Flow rates are: (a) 200 μl/h, (b) 150 μl/h, (c) 100 μl/h, and (d) 80 μl/h.

A relatively modest level of multiplexing, that is, with a number of ESs no larger than 19, was chosen to ease the debugging of the system. By preserving nozzle dimensions, inter-nozzle pitch and the same average flow rate for each nozzle, scale-up by at least three orders of magnitude is feasible from a single 4-in. wafer, which will result in particle production rates in excess of 10 g/h.

4. Conclusions

We developed a well-controlled method to generate PLGA microparticles of different morphologies by electrospray drying. The final morphology is based on the relative importance and sequence of occurrence of Coulomb fission and polymer entanglement, which can be controlled a priori by judiciously selecting polymer molecular weight, concentration and solution flow rate. Principal conclusions follow:

1. Spherical particles are generated when a sufficiently entangled network is formed prior to the onset of the Rayleigh limit in the droplets. Elongated and tailed particles, potentially more advantageous for drug delivery purposes, are obtained otherwise.
2. Control of particle morphology (from spherical to non-spherical) is achievable for polymer solutions with concentrations bound between two limits: a lower one for entanglements to set in and an upper limit beyond which fibers are generated in the breakup region of the spray. The range of this concentration becomes narrower with increasing polymer molecular weight.
3. An extension of a simple model, originally used to determine the onset of electrospinning of polymer solutions, adequately sorts out conditions leading to either spherical or non-spherical products from a priori knowledge of a few solution properties and flow rate.
4. These findings are confirmed in experiments at larger flow rate with multiplexed ES sources, which addresses the notorious low-throughput limitation of the electrospray drying method.

Acknowledgments

Appendix A. Supplementary material

Supplementary data associated with this article can be found, in the online version, at doi:10.1016/j.jcis.2009.10.002.

References

[1] R.A. Jain, Biomaterials 21 (2000) 2475.
[2] M.L. Hans, A.M. Lowman, Curr. Opin. Solid State Mater. Sci. 6 (2002) 319.
[3] R.M. Mainardes, L.P. Silva, Curr. Drug Targets 5 (2004) 449.
[4] T.M. Fahmy, P.M. Fong, A. Goyal, W.M. Saltzman, Mater. Today 8 (2005) 18.
[5] S.M. Moghimi, A.C. Hunter, J.C. Murray, Pharmacol. Rev. 53 (2) (2001) 283.
[6] O.C. Farokhzad et al., PNAS 103 (16) (2006) 6315.
[7] R. Sinha et al., Mol. Cancer Ther. 5 (8) (2006) 1909.
[8] H. Takeuchi, H. Yamamoto, Y. Kawashima, Adv. Drug Delivery Rev. 47 (1) (2001) 39.
[9] S.H. Kim, Langmuir 21 (19) (2005) 8852.
[10] T.M. Fahmy et al., Aaps J. 9 (2) (2007) E171.
[11] J.A. Champion, Y.K. Katare, S. Mitragotri, J. Control Reliab. 121 (2007) 3.
[12] E.A. Simone, T.D. Dziubla, V.R. Muzykantov, Expert Opin. Drug Delivery 5 (12) (2008) 1283.
[13] D.S.T. Hsieh, W.D. Rhine, R. Langer, J. Pharm. Sci. 72 (1) (1983) 17.
[14] Y. Geng, P. Dalhaimer, S. Cai, et al., Nat. Nanotechnol. 2 (4) (2007) 249.
[15] E.A. Simone, T.D. Dziubla, D.E. Discher, V.R. Muzykantov, Biomacromolecules 10 (2009) 1324.
[16] J.A. Champioon, S. Mitragotri, PNAS 103 (13) (2006) 4930.
[17] S.E.A. Gratton, P.A. Ropp, P.D. Pohlhaus, et al., PNAS 105 (33) (2008) 11613.
[18] S. Muro, C. Garnacho, J.A. Champion, et al., Mol. Ther. 2008 (1450).
[19] J. Xie, C. Wang, Biotechnol. Bioeng. 97 (2007) 1278.
[20] J. Xie, L.K. Lim, Y. Phua, J. Hua, C. Wang, J. Colloid Interface Sci. 302 (2006) 103.
[21] J. Yao, L. Kuang Lim, J. Xie, J. Hua, C. Wang, J. Aerosol Sci. 39 (2008) 987.
[22] Y. Hong, Y. Li, Y. Yin, D. Li, G. Zou, J. Aerosol Sci. 39 (2008) 525.
[23] C.J. Hogan Jr., K.M. Yun, D. Chen, I.W. Lenggoro, P. Biswas, K. Okuyama, Colloids Surf. A 311 (2007) 67.
[24] I.W. Lenggoro, T. Hata, F. Iskandar, M.M. Lunden, K. Okuyama, J. Mater. Res. 15 (2000) 733.
[25] K. Okuyama, I.W. Lenggoro, Chem. Eng. Sci. 58 (2003) 537.
[26] R. Vehring, W.R. Foss, D. Lechuga-Ballesteros, J. Aerosol Sci. 38 (2007) 728.
[27] C.H. Park, J. Lee, J. Appl. Poly. Sci. 114 (2009) 430.
[28] F. Meng, Y. Jiang, Z. Sun, Y. Yin, Y. Li, J. Appl. Polym. Sci. 113 (2009) 526.
[29] S.L. Shenoy, W.D. Bates, H.L. Frisch, G.E. Wnek, Polymer 46 (2005) 3372.
[30] D. Chen, D.Y.H. Pui, J. Aerosol Sci. Technol. 27 (1997) 367.
[31] J. Rosell-Llompart, J. Fernández de la Mora, J. Aerosol Sci. 25 (1994) 1093.
[32] J. Fernández de la Mora, I.G. Loscertales, J. Fluid Mech. 260 (1994) 155.
[33] W. Deng, J.F. Klemic, X. Li, M.A. Reed, A. Gomez, J. Aerosol Sci. 37 (2006) 696.
[34] W. Deng, C.M. Waits, B. Morgan, A. Gomez, J. Aerosol Sci. (2009).
[35] W. Deng, A. Gomez, J. Aerosol Sci. 38 (2007) 1062.
[36] A. Gomez, K. Tang, Phys. Fluids 6 (1994) 404.
[37] L. Rayleigh, Philos. Mag. 14 (1882) 184.
[38] R. Festag, S.D. Alexandratos, D.C. Joy, B. Wunderlich, B. Annis, K.D. Cook, J. Am. Soc. Mass Spectrom. 9 (1998) 299.
[39] P.G. De Gennes, Scaling Concepts in Polymer Physics, Cornell University Press, Ithaca, 1979.
[40] Y. Wu, J.A. MacKay, J.R. McDaniel, A. Chilkoti, R.L. Clark, Biomacromolecules 10 (2009) 19.
[41] C. Berkland, D.W. Pack, K.K. Kim, Biomaterials 25 (2004) 5649.
[42] J. Fernández de la Mora, J. Colloid Interface Sci. 178 (1996) 209.
[43] D. Chen, D.Y.H. Pui, S.L. Kaufman, J. Aerosol Sci. 26 (1995) 963.